Pergamon

Journal of Structural Geology, Vol. 16, No. 10, pp. 1353 to 1365, 1994

0191-8141/94 $7.00 + 0.00

0191-8141(94)E0007-L

Strain, cleavage and microstructure variations in sandstone: implications for stiff layer behaviour in chevron folding

XINYUE YANG

Changsha Institute of Geotectonics, Academia Sinica, Changsha, Hunan 410013, People's Republic of China

and

DAVID R. GRAY

Department of Earth Sciences, Monash University, Melbourne, Victoria 3168, Australia

(*Received* 19 *May* 1992; *accepted in revised form* 4 *January* 1994)

Abstract—Sandstone layers within tightly chevron-folded quartz-rich turbidites of the Lachlan Fold belt southeastern Australia show a fanning spaced cleavage overprinted by a non-fanning grain alignment cleavage, low internal strains recorded by quartz grain separations ($XZ \approx 1.4$–1.8) and low fold flattening strains ($XZ < 1.8$). Angular relations between spaced cleavage and bedding in folds with varying tightness suggest that sandstone layers initially act as stress-supporting members with spaced cleavage development due to pressure solution taking place at limb dips up to 15°. During fold development sandstone layers undergo rigid body rotation involving interlayer slip without marked internal deformation except at fold hinges. After fold lock-up bedding–spaced cleavage angles change due to inner arc collapse by pressure solution and subsequent flattening with formation of a grain alignment cleavage and mica beard growth. Internal deformation of sandstone is characterized by microstructures related to solution–redeposition processes and growth of mica. Chevron folds form by homogeneous shortening and pressure solution due to layer-parallel shortening, tangential longitudinal strain due to buckling, fold tightening by inner arc collapse due to pressure solution and fold flattening at metamorphic peak with growth of mica. Geometric modelling of internal strains and bedding–cleavage angles requires a significant component of interlayer slip during chevron fold development under greenschist facies conditions.

INTRODUCTION

MICROSTRUCTURES, strain patterns and geometric relationships between folds and cleavage within folded rock layers are important for understanding the process of folding and the deformation mechanisms within and between deformed rock layers during folding (e.g. Groshong 1975, Boulter 1979, Gray 1981, Onasch 1990). In this paper, we examined cleaved sandstone layers within a tightly folded turbidite sequence to see how folded sandstone layers form tight to almost isoclinal chevron folds.

Theoretical and experimental investigations on chevron-fold development have shown that stiff layers have a strong influence on the development of folds within multilayer systems (Paterson & Weiss 1966, Ghosh 1968, Dieterich & Carter 1969, Johnson 1977). In the early stages of folding stiff layers act as struts supporting the stress, but as the buckling instabilities amplify and propagate, these layers passively rotate accompanied by interlayer slip and/or deformation within the weak layers (i.e. flexural-flow). Buckling ceases at interlimb angles approaching 60–65° with lock-up and fold flattening takes over accompanied by hinge collapse, and the development of limb thrusts and saddle reefs (De Sitter 1956, Ramsay 1974). Both the multilayer thickness ratio (t_1/t_2, where t_1 is the stiff and t_2 the weak layer thickness, respectively) and the contact strength between layers control the buckling instability (e.g. Ghosh 1968, Johnson 1977).

Internal deformation can occur within the stiff layers during the folding process (e.g. Chapple & Spang 1974, Nakahara & Wiltschko 1986). At low metamorphic grade this results in the formation of a spaced cleavage within the sandstone layers of folded sandstone–mudstone sequences. This cleavage usually develops as systematic fans such that the geometric relationship between the cleavage and folds can be used to establish the timing and sequence of cleavage development relative to folding (cf. Boulter 1979, Gray 1981). At the grain scale, microstructure can also be used to track the processes involved in fold development (e.g. Mitra 1978). Cleavage in deformed sandstone results from an interplay between pressure solution, mica growth and fracturing deformation mechanisms (Means 1975, Gray 1978, Onasch 1983, 1990, Wu & Groshong 1991). The relative role of these processes is important in determining sandstone layer behaviour during chevron folding.

In this study determination of strain at the grain scale within sandstone layers was carried out utilizing object–object separation methods on quartz grains (e.g. Fry 1979, Hanna & Fry 1979). These are useful in depicting grain spacing modifications related to tectonic fabric development (cf. Onasch 1986). Patterns of strain in the

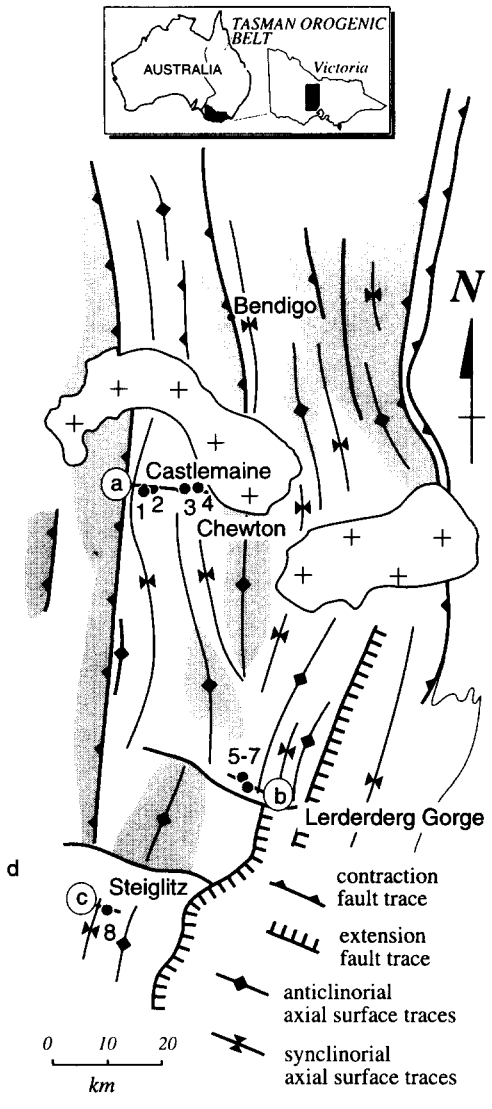

Fig. 1. Regional map of part of the Bendigo–Ballarat structural zone showing the major geological elements including Late Devonian post-tectonic granitoids (crosses) and the outcrop pattern of Lancefieldian (lowermost Lower Ordovician) quartz-rich turbidites (shaded). Outcrop traces of major faults and anticlinorial and synclinorial axial surface traces are also shown (modified from Gray & Willman 1991b, fig. 1). Numbered dots represent the locations of folds studied in this paper (see Appendix 1). Positions of the section lines in Fig. 2 are shown as circled lower case letters; **a** (Chewton–Castlemaine), **b** (Lerderderg gorge) and **c** (Steiglitz).

chevron-folds studied in this paper have been mapped for different sandstone layers and used to establish the mode of folding and the overall behaviour of sandstone layers in the folding process (e.g. Hudleston & Holst 1984).

This paper investigates the behaviour of stiff layers in the chevron-folding process by examining: (1) aspects of sandstone microstructure; (2) strain within the sandstones recorded by changes in object–object separation distances (Fry method); (3) changes in the bedding–cleavage angles ($S_0 \wedge S_1$) with increasing fold tightness; and (4) and fold flattening using a modified $t'\alpha$ analysis. The sandstones investigated are from the upper parts of thrust sheets within the Bendigo–Ballarat zone of the Lachlan fold belt, southeastern Australia (Fig. 1). They are part of an extensive low greenschist facies quartz-rich sandstone and interlayered mudrock sequence (Gray 1988, Gray *et al.* 1991). The outcrops and folds are from Castlemaine–Chewton (folds 1, 2, 3 and 4), Lerderderg Gorge (folds 5, 6 and 7) and Steiglitz in the Brisbane Ranges (fold 8) (see Fig. 1 and Appendix 1).

GEOMETRY AND ASSOCIATION OF CHEVRON FOLDS

Chevron folds with interlimb angles ranging from 35° to 50° occur in the upper parts of thrust sheets characterized by some 50–65% shortening (cf. Gray & Willman 1991a, b). Fold axial surface traces are subparallel to major fault traces and folds are cut by both E- and W-dipping reverse faults (Fig. 2). Fault displacements tend to be small and as such the overall shortening due to faulting tends to be <5% (Gray & Willman 1991a, table 1). Such faults have been interpreted as accommodation structures during late stage shortening (Gray & Willman 1991a, b, Cox *et al.* 1991). Mudstones interbedded with the sandstones are cleaved, have low strains (*XZ* strains < 5.0:1) and have undergone subvertical extension shown by straight quartz-fibres in pressure shadows on framboidal pyrite.

Folds within sandstone layers are gently plunging, upright, angular forms with long planar limbs and narrow hinge zones (Fig. 2). At the outcrop scale they have somewhat rounded hinges and class 1C (Ramsay 1967) geometry (Fig. 3a). Chevrons occur as extremely regular fold trains with 200–300 m wavelengths and 50–100 m amplitudes. Thickness–curvature relationships (t/r, where t = bed thickness and r = radius of bed curvature; see Donath & Parker 1964) for sandstone layer folds range from 0.27–0.59 (class 1B folds) to 1.0–1.35 (class 1C folds). Bedding parallel veins, saddle reefs and laminated fault-fill veins are associated with the chevron folds (Cox *et al.* 1991, Gray *et al.* 1991, Jessell *et al.* in press).

CLEAVAGE IN FOLDED SANDSTONE LAYERS

Sandstone layers (Fig. 3b) show a widely spaced (2–5 cm) spaced cleavage with thick micaceous selvages overprinted by a finely spaced (<2 mm spacing) grain alignment cleavage (Figs. 3c & d). A cm-scale spaced cleavage of crenulation form occurs in plane laminated sandstone (Bouma B beds), cross-laminated sandstone (Bouma C beds) and laminated mudstones (Bouma D beds) of individual turbidite packages or Bouma sequences (Fig. 3e). Spacing of cleavage varies markedly with position on folds; in the limbs and outer arc of folds cleavage spacing is usually 1–4 cm but in the inner arc cleavage is much more pervasive with intercleavage distance of <1 cm (Figs. 3a & b). Consequently, sandstone in the inner arc of folds has a much better fissility than that on the limbs and in the outer arc.

Sandstone fabrics at the grain scale are influenced by quartz–grain alignment (Figs. 4b & c), spaced stylolitic

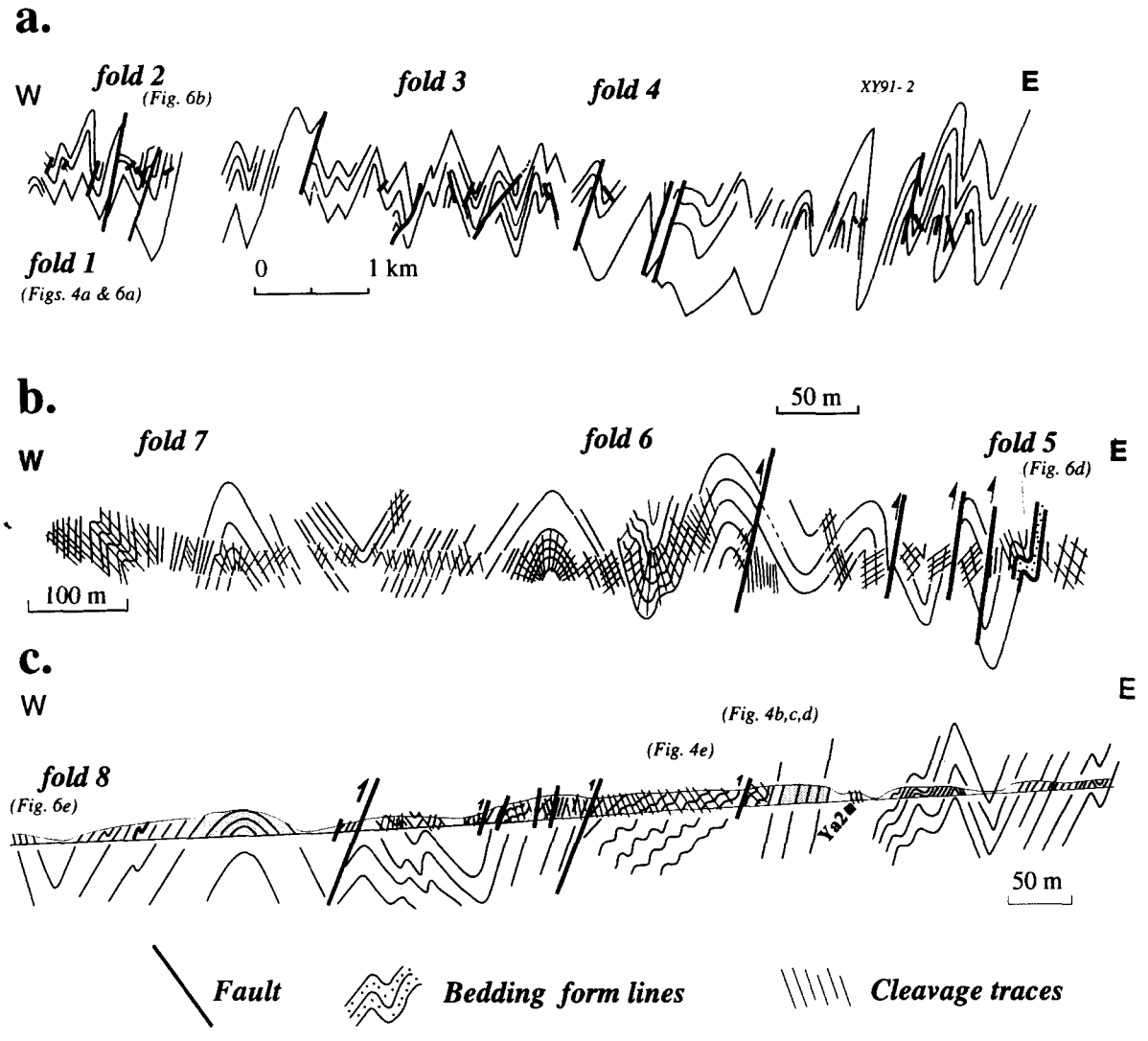

Fig. 2. Typical geometry of chevron-folded interlayered sandstone–mudstone turbidite sequences shown in structural profiles (for locations see Fig. 1). (a) Castlemaine–Chewton section (modified from Cox *et al.* 1991); (b) Lerderderg Gorge section. (c) Steiglitz–Moorabool River road section. Positions of folds analysed in this paper and outcrop photographs are shown.

cleavage seams (Fig. 4b) and mica beard fabrics in the matrix (Figs. 4f & e). The cleavage traces are layer silicate films usually 15–40 μm in width and defined by very fine mica and opaques. Many of the sandstones particularly those transitional between Bouma A and B layers show an alignment of elongate quartz grains and detrital micas parallel to bedding (Fig. 4f); detrital mica constitutes up to 5% of some sandstones. Weak cleavage is defined by weakly developed mica beards and layer silicate films around detrital quartz grains with aspect ratios typically between 1:1 and 3:1. In hinge zones strongly aligned, long, splinter-like quartz grains with sutured irregular boundaries typically have aspect ratios between 5:1 and 10:1 and are enveloped by thick layer silicate films.

In the inner arcs of some of the mesoscopic folds syntectonic crack–seal fibrous quartz veins indicate a component of vertical extension parallel to cleavage. Microveins (vein thicknesses <100 m) and fracture boudinage of opaques indicate that vertical extensional strains of at least 10–30 are associated with cleavage development (Fig. 4d).

CLEAVAGE–FOLD RELATIONSHIPS

Cleavage fanning

Spaced cleavage in sandstone layers shows systematic convergent fanning in profile-section of mesoscopic folds (Figs. 2 and 5). In class 1C–1B (Ramsay 1967) folds in which the dominant rock is sandstone and/or sandstone with interlayered mudrock the interlimb angles are from 36° to 80° and cleavage fan angles are from 62° to 116° (see Appendix 1). Analysis of interlimb angle (α) and cleavage fan angle (β) data for some sandstone layer folds shows that the cleavage fan angle increases with increasing fold tightness (Fig. 6a); the best-fit line for sandstone is $\beta + 0.69\alpha = 122°$ (correlation coefficient $R = 0.84$; sample size $n = 19$). Mudstones interbedded with the sandstones have class 3/2 geometry (Ramsay 1967), interlimb angles of 36–90° and cleavage fan angles of 25–58° (Appendix 1). For mudstone the best-fit line is $\beta + 0.4\alpha = 63°$ (correlation coefficient $R = 0.8$; sample size $n = 6$).

On tightness vs fan angle graphs (Fig. 6a) the line $\alpha +$

$\beta = 180°$ line tracks the rigid-body (passive) rotation of a marker originally normal to bedding (see Gray 1981). Points along this line indicate the progressive changes to cleavage fan angle with tightening of folds.

Cleavage and bedding relationship

Sandstones show a variation in $S_0 \wedge S_1$ but most angles are $> 60°$ (Fig. 6b); cleavage is at a high angle to bedding even in nearly vertical limbs. They show a high scatter on plots of $S_0 \wedge S_1$ (ϕ) against limb dip (θ), but $S_0 \wedge S_1$ generally decreases with increasing limb dip (Fig. 6b); for sandstone $\phi + 0.19\,\theta = 78.4°$ (correlation coefficient $R = 0.3$; sample size $n = 19$).

Bedding–cleavage angles ($S_0 \wedge S_1$) in mudrock layers have much greater variation (5–85°) than in sandstone (Fig. 6b). $S_0 \wedge S_1$ in mudrock decreases sharply with increasing limb dip (Fig. 6b); the best-fit line for mudstone is $\phi + 1.6\,\theta = 148.6°$ (correlation coefficient $R = 0.7$; sample size $n = 14$).

STRAIN PATTERNS IN SANDSTONE LAYERS

Method

The Fry method (Fry 1979, Hanna & Fry 1979) was used to determine bulk strain within sandstone layers using quartz grain centre separations (cf. Crespi 1986, Onasch 1986). Centre-to-centre spacings of neighbour quartz grains in the deformed state are a function of the direction and magnitude of strain. Because the Fry method was developed as a simple graphical method to measure strains from homogeneously deformed anticlustered strain markers, the degree of anticlustering, size and shape variations of quartz grains and inhomogeneous deformation can influence the results (Lacassin & Van den Driessche 1983; Crespi 1986, Onasch 1986, Dunne *et al.* 1990).

Measurements were carried out from photomicrographs of thin sections cut parallel and perpendicular to the principal fabric elements in the sandstones. Centres of quartz grains were digitized and then input into program 'Instrain' (written by Eric Erslev, Rockware Inc. 1989). Strain magnitudes and principal stretch directions were calculated from either vacancy and/or high density ellipses from conventional Fry plots (Fig. 7), although normalized and/or enhanced methods were used depending on the strength and definition of the vacancy ellipse (cf. Erslev 1988). All of the samples were from intercleavage zones between the fanning spaced cleavages.

Results

Strength and definition of the vacancy ellipse, as well as type and number of ellipses varied with sandstone fabric (Fig. 7 and Appendix 2). Sandstones containing moderate to strong grain alignment cleavage generally showed a vacancy ellipse and/or high density ellipse parallel to the grain alignment (Figs. 7a & b). Sandstones with weaker grain alignment cleavage and a proportion of elongate grains (aspect ratios >3:1) parallel to bedding, either showed an ill-defined vacancy ellipse parallel to the grain alignment cleavage (Fig. 7c), or two superimposed vacancy ellipses, one parallel to bedding and the other subparallel to the grain alignment cleavage (see Appendix 2; cf. Lacassin & Van den Driessche 1983).

Because samples are from sandstone between the spaced cleavage, strains determined from Fry plots of quartz grain centre spacings generally reflect strains associated with development of the grain alignment cleavage. Although the strength and definition of both vacancy and density ellipses varied considerably the magnitudes and directions of principal strains were remarkably consistent (see Appendix 2). Patterns and magnitudes of strain recorded by detrital quartz grain object–object separations within sandstone layer folds are generally low (1.1–1.8) and show consistent relationships in strain magnitude and direction around chevron folded sandstone layers (Fig. 5).

Relation to chevron folds

The folds analysed (folds 1, 2, 3, 5 and 8, Fig. 1) have varying tightness; interlimb angles are 89°, 80°, 80°, 45° and 36°, respectively (see Appendix 1). Strain analysis of these chevron-folded sandstone layers has shown that:

(1) strain magnitudes in fold inner arcs are higher than in the outer arc and limbs (Figs. 5b, d & e);

(2) in the more open folds XZ strains are relatively homogeneous (Fig. 5a) and may represent positions close to the neutral surface where R values approach 1;

(3) determined principal X stretch directions in the inner arc are always consistent with cleavage traces in profile-section whereas XZ ellipses are aligned parallel to the bedding traces in the outer arcs of folds (Figs. 5c & e);

(4) in the fold limbs there is obliquity of determined X directions with spaced cleavage trajectories (Figs. 5a & e). Vacancy ellipses are subparallel to a weak grain alignment cleavage;

(5) tight folds with steep limbs show grain alignment cleavage intersecting with bedding parallel fabrics where the determined X direction is parallel to the grain alignment cleavage (Figs. 5d & e).

MECHANISMS OF FOLDING

What do the sandstone layers in tight chevron folds record about the folding process? These sandstone layers show low internal strains ($R < 1.8$; Appendix 2) whose magnitudes are comparable to the determined fold flattening strains ($R_{fl} < 1.8$; Appendix 1). The strains are so low that bedding fabrics are still preserved in most of the sandstones. Thickness changes are small but noticeable within the hinges of sandstone layer folds. Cleavages are typically of the spaced variety and are

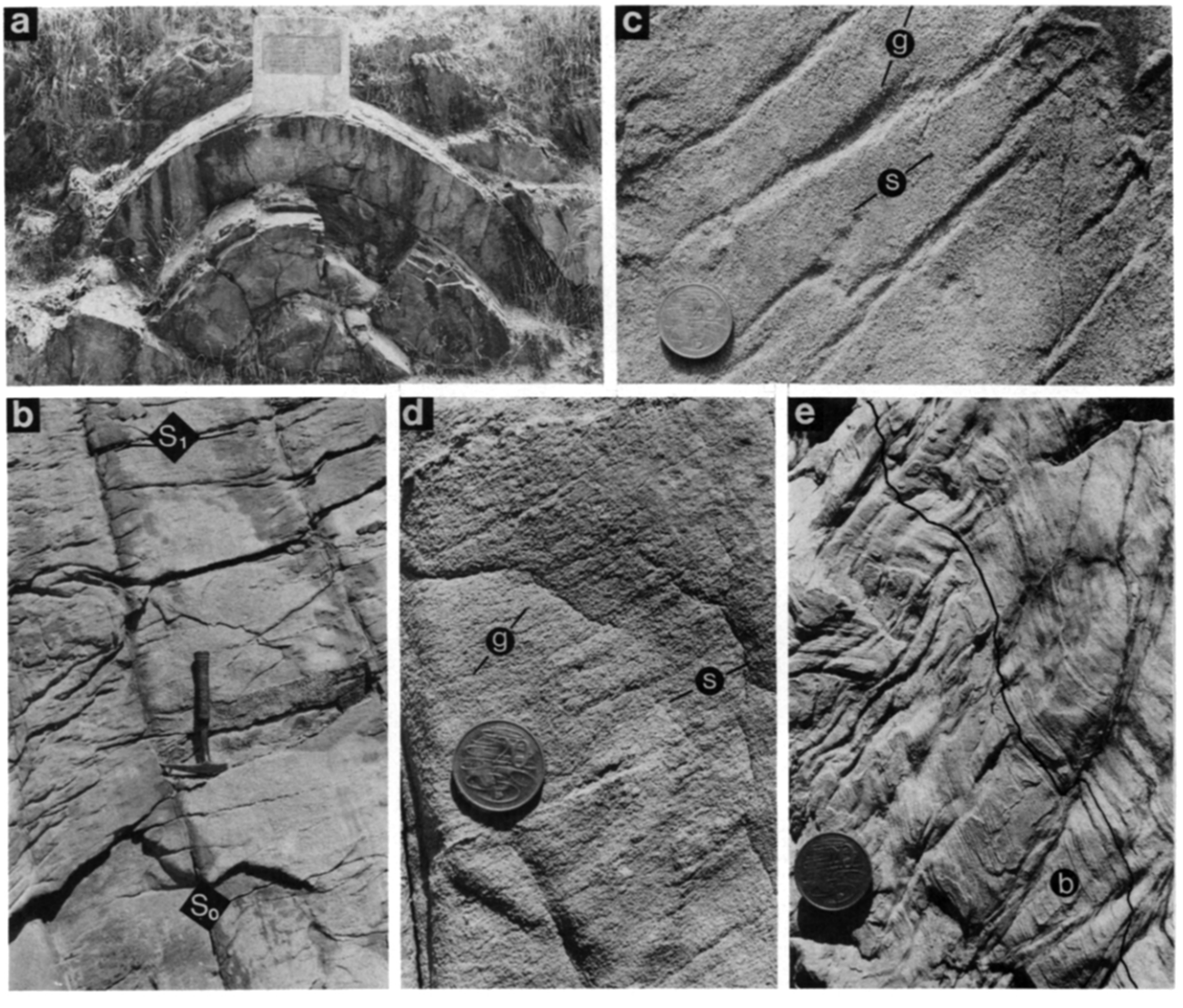

Fig. 3. Structures in sandstone sequences. (a) Rounded anticlinal hinge in road cutting, Castlemaine (fold 2, Appendix 1). (b) Homoclinally dipping sandstone beds showing variations in the intensity of spaced cleavage development. Road cutting exposure near Steiglitz, Brisbane Ranges. (c) Spaced cleavage zones (s) in sandstone. Weathering has enhanced these cleavage zones as lenticular pits with resistant quartz grains in the intercleavage zones highlighting the grain alignment fabric (g). (d) Intersecting grain alignment cleavage (g) and weak spaced cleavage (s) in sandstone layer; road cutting near Steiglitz, Brisbane Ranges. (e) Box-like folds (b) and kink-like crenulations in plane-laminated sandstone. Road cutting, near Steiglitz. Diameter of Australian 20 cent coin in (c), (d) and (e) is 2.8 cm.

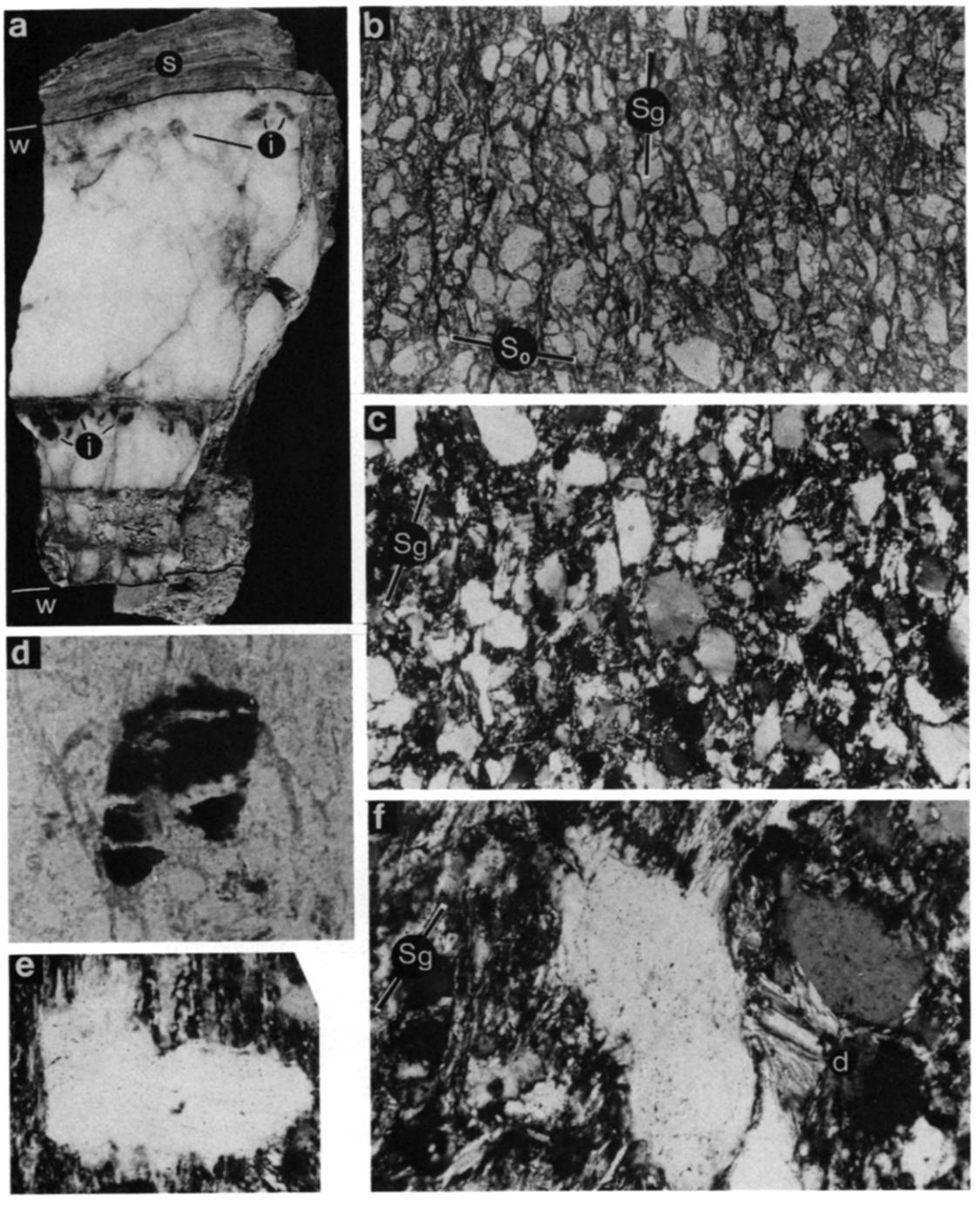

Fig. 4. Bedded vein morphology (a) and microstructural features of rough cleavage in sandstone (b–f). (a) Section across a 14 cm thick bedded vein showing a 2 cm thick laminated wall-rock selvage (s) where slip is considered to have taken place during chevron folding. The vein is composed of massive, milky white recrystallized quartz with remnants of the former (i.e. pre-recrystallization) bedded vein microstructure preserved as dark inclusions (i); w, wall of vein; Little Bendigo, Castlemaine region. (b) Photomicrograph of grain alignment fabric (S_g) showing discontinuous, cleavage seams with little development of mica beards. Cleavages are dark irregularly oriented phyllosilicate films with lengths greater than individual grains. Strain ratio $R = 1.8$ based on Fry analysis of quartz grains. Base of photograph is 4 mm (sample XY91-7B2). (c) Cleaved sandstone fabric showing weak grain alignment (S_1) and weak to moderate alignment of phyllosilicates in the matrix. Healed microfractures are rare and there is no evidence of recrystallization within the detrital quartz grains. Strain ratio $R = 1.7$ based on Fry analysis of quartz grains. Crossed nicols view. Base of photograph is 4 mm (sample XY91-7C2). (d) Photomicrograph of pull-apart (microboudinage) of opaque minerals within a cleavage parallel section. Reconstruction of the opaques indicates 11% subvertical extension within the plane of the cleavage. Base of photograph is 300 μm (sample XY91-7C1). (e) Photomicrograph of mica beard structure around a detrital quartz grain showing quartz overgrowth and a strong growth alignment of the impinging micas. Section is parallel to cleavage. Cross nicols view. Base of photograph is 700 μm (sample XY91-5C1). (f) Photomicrograph showing strong mica alignment in the groundmass, mica beard development and a relict detrital mica aligned subparallel to S_0 (d); S_1, cleavage trace. Cross nicols view. Base of photograph is 1.2 mm (sample XY91-5C2).

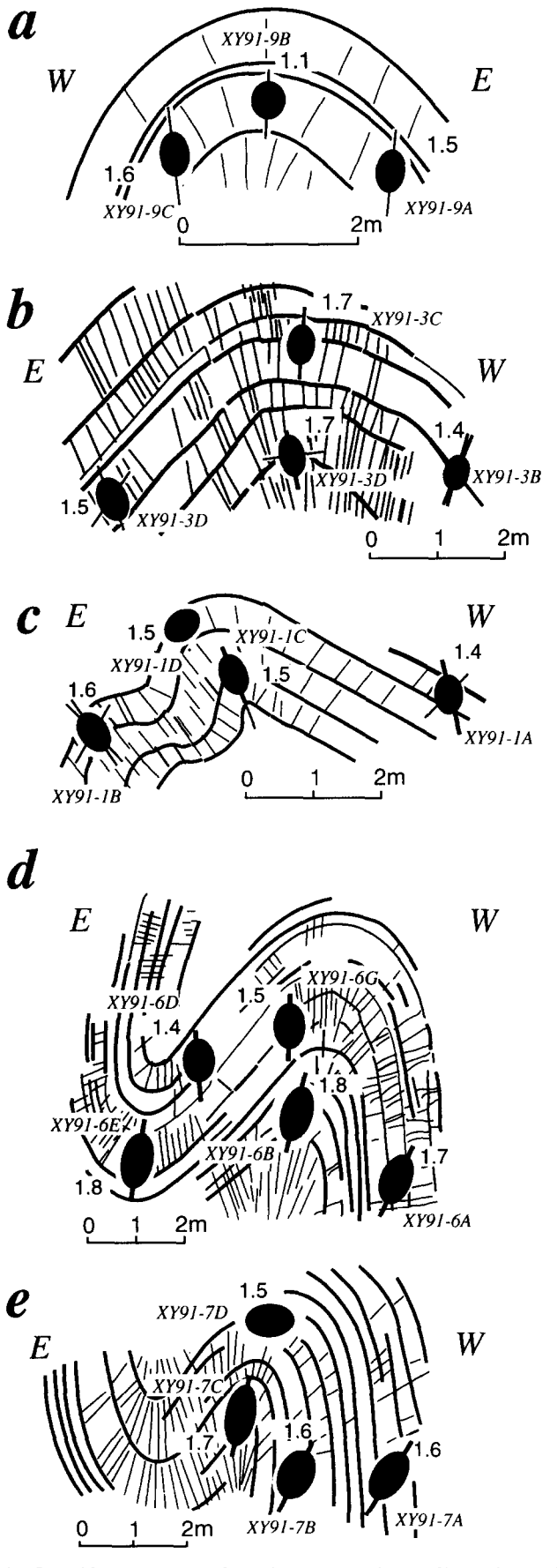

Fig. 5. Fold geometry and strain patterns in profile-sections of selected sandstone layer folds (see Appendix 1); locations of folds are shown in Fig. 1. The orientations and magnitudes of XZ strain ellipses were determined by modified Fry analysis of quartz grain populations from thin sections (see Appendix 2). (a) Fold No. 1, Castlemaine; (b) fold No. 2, Castlemaine; (c) fold No. 4, Chewton; (d) fold No. 5, Lerderderg Gorge; (e) fold No. 8, Steiglitz, Brisbane Ranges.

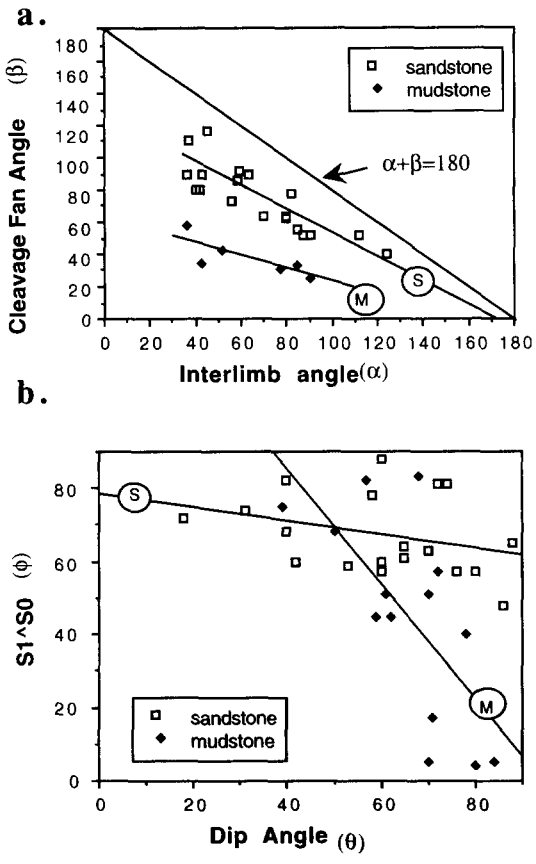

Fig. 6. Graphs of cleavage–fold relationships for chevron-folded sandstone layers. Square symbol, data from sandstone folds; solid diamonds, data from mudstone folds (a). Interlimb angle (a) plotted against cleavage fan angle (b); S ($\beta = -0.7\alpha + 121.6$; $R = 0.84$) and M ($\beta = -1.6\alpha + 148.7$; $R = 0.67$) lines are best-fit lines correspond to sandstone and mudstone data, respectively. (b) Limb dip vs bedding–cleavage angle ($S_0 \wedge S_1$); S ($\phi = -0.2\theta + 78.4$; $R = 0.35$) and M ($\phi = -1.6\theta + 148.7$; $R = 0.67$) lines are best-fit lines correspond to sandstone and mudstone data, respectively.

fanned about the folds, but are cut by a younger grain alignment cleavage which is parallel to fold axial surfaces. Cleavage is best developed within the inner arcs of folds.

Behaviour of the intervening mudstone layers and the relative amounts of slip along bedding surfaces is also crucial to multilayer folding. In the rocks investigated cleavage trajectory patterns, fibre patterns in pressure shadows and the presence and significance of bedded veins are also important to understanding how the chevron folds developed in these sandstone/mudstone multilayers. Each of these aspects will now be addressed.

Implications of two cleavages in one folding event

Superimposed spaced and grain alignment cleavages formed during one folding event have been recognized in sandstone–slate sequences (Harris *et al.* 1976, fig. 2, Boulter 1979, fig. 5, Powell & Rickard 1985). The grain alignment cleavage is always more axial planar to the folds and has formed late in the folding sequence.

The presence of these superimposed cleavages re-

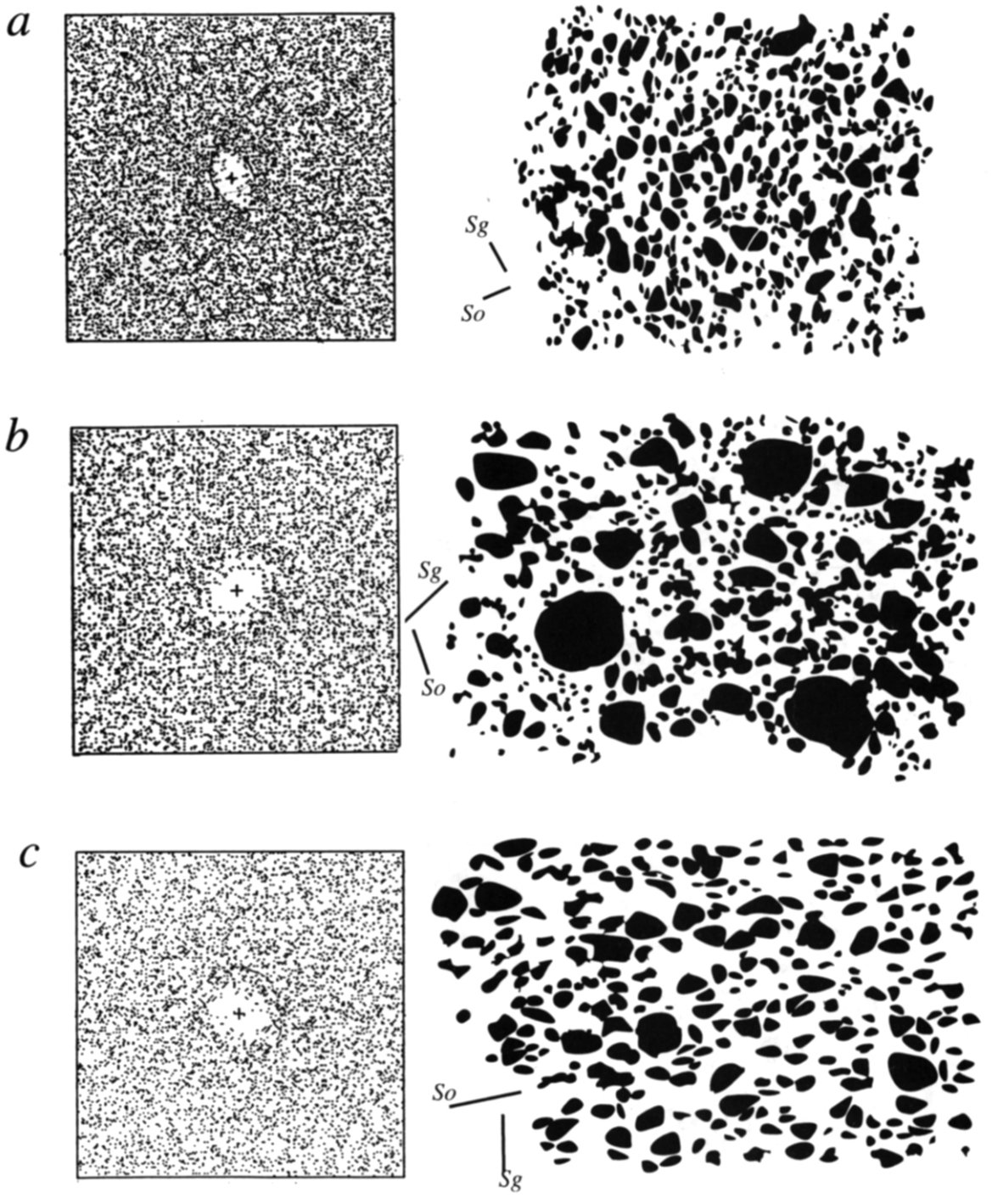

Fig. 7. Fry plots of typical quartz grain distributions imaged from photomicrographs of chevron-folded sandstone layers. Sections are all cut perpendicular to cleavage and the bedding–cleavage intersection lineation. (a) Sandstone with reasonable sorting showing elongate grains both subparallel to bedding and grain alignment cleavage (sample XY91-3C2: fold 2 hinge, Castlemaine; Fig. 6b). Fry plot shows a vacancy ellipse parallel to the grain alignment cleavage with a 1.7 axial ratio. (b) Poorly sorted sandstone with low quartz grain preferred orientations (sample XY91-3D2: fold 2 limb; Castlemaine; Fig. 6b). Fry plot shows subparallel, superimposed vacancy and density ellipses with axial ratio of 1.5. (c) Strong alignment of quartz grains parallel to bedding in sandstone (XY91-9B2: fold 1 hinge, Castlemaine; Fig. 6a). Fry plot shows density ellipse with 1.1 axial ratio parallel to a weak grain alignment cleavage.

quires a change in the deformation conditions from the early to late stages of folding, from that dominated by dissolution of quartz to that of mica growth accompanied by dissolution and reprecipitation of quartz. Marked mica and beard growth occurred during development of the grain alignment cleavage, coincident with the peak of metamorphism and attainment of maximum structural thickness. During the early folding increments, prior to significant buckling, spaced cleavage development was by pressure solution with little or no mica growth. However, the effects of pressure solution are not homogeneous and intensity of dissolution varies with position in folds; effects including grain shape changes, cleavage selvage thickness and extension veining are greater in the inner arc of folds than in the outer arc and limbs.

Implications of bedding–cleavage relationships

Changes in cleavage fan angle within sandstone layers reflect the limb rotation and the internal strain within the layers (cf. Boulter 1979, Gray 1981). The observed changes (Fig. 7a) indicate that the folding approximates bending or tangential longitudinal strain with the spaced cleavage being initiated at interlimb angles between 170° and 180° and progressively fanned during limb rotation. Chevron-fold data follow a trend subparallel to the line $\alpha + \beta = 180°$ with an intercept of 170°. Fold flattening has no pronounced effect on the fan angle unlike cleaved sandstone and limestone layers from folds in the Virginia Appalachians where increasing fold tightness (100–50°) was accompanied by a decrease in fan angle (see Gray 1981, fig. 5a). The sandstone cleavage data indicates that fold flattening strains (layer thickness changes) within sandstone must have occurred as increments during the folding process rather than as a separate event late in folding (cf. Hudleston 1973).

Changes in bedding–cleavage angle reflect both the timing of cleavage development in the folding process (i.e. this determines the initial $S_0 \wedge S_1$) and the internal strain within the sandstone host. The initial angle within sandstone layers is approximately 80° for low limb dips $\theta = 0$–10° and changes to 60–65° for limb dips approaching 75° (see Fig. 7b). This change in $S_0 \wedge S_1$ indicates that sandstone layers have undergone shape and fabric modifications at the grain scale during the folding process.

Implications of sandstone layer strains

Idealized strain patterns of folds in stiff layers include tangential longitudinal strain, flexural flow, inner arc collapse due to pressure solution and volume loss, and homogeneous strain plus inner arc collapse (cf. Hudleston & Holst 1984, fig. 7). The observed strain pattern of extension in the outer arc and shortening in the inner arc of tight folds is typical of tangential longitudinal strain (Ramsay 1967, fig. 7-63), despite the fact that the strains determined from grain centre separations should reflect the superimposed strains from compaction (cf. Boulter 1976), tangential longitudinal strain and fold flattening.

Homogeneous and lower magnitudes of strain in more open folds (Fig. 6a) suggests samples here are close to the former neutral surface. The lack of extension veins in the outer arc of most folds suggests that tensile failure in the outer arc beyond the neutral surface was counteracted to some extent by material adjustment due to pressure solution and reprecipitation in the inner arc (inner arc collapse).

Fracturing preserved as subhorizonal veins and microveins contributes to a subvertical extension within the sandstone layers. Microboudinage of opaques (Fig. 4d) indicates that microfracturing makes up 10–30% of this bulk extension. Lack of extension parallel to fold axes during folding suggests plane strain deformation, and agrees with observations on pressure shadows and strain determinations on deformed graptolites in the intervening mudstone layers (see Gray & Willman 1991b).

Implications of the mudstone layers

Low strains in the sandstones would argue for either flexural-flow within the intervening mudstone layers or significant component of flexural-slip along some bedding surfaces. Fabric development within the mudstones is not due to flexural-flow but has been related to flattening increments late in folding (Gray & Willman 1991a & b). This is because fibres in pressure shadows in mudrock layers are always straight and subvertical, independent of their position in chevron folds. Straight fibres require coaxial deformation increments such as fold-flattening. Approximately simultaneous increments of flattening and buckling to achieve the final fold shapes in mudstone layers (Hudleston 1973) should produce curved fibres in pressure shadows along fold limbs (cf. Beutner & Diegel 1985). These are clearly not observed.

Retro-deformation of chevron-fold trains by removal of strains within mudrock layers suggests that cleavage development in pelites occurred after chevron-folds had attained interlimb angles of approximately 90° (see Gray & Willman 1991b, fig. 10c). This means that strain accumulation in pelites as recorded by syn-tectonic fibre growth in pressure shadows, and presumably cleavage development as well, was suppressed until limb dips of approximately 45° had been achieved. Frictional resistance to layer-parallel slip may have occurred at this stage with subsequent shortening due to fold-flattening, largely by cleavage development in the intervening pelites and the development of hinge accommodation structures.

Implications of bedding-parallel veins

Bedding-parallel veins are common in chevron-folded sequences and here have been attributed to dilational stick–slip development in the pre-buckling stages of folding where movement is controlled by fluctuations in pore fluid pressure (Jessell *et al.* in press). A pre-folding origin is suggested by vein opening sense unrelated to the flexural folds which eventually fold them. These veins are also buckled, cut by the spaced cleavage and undergo recrystallization in fold hinges.

Slickensided wall-rock selvages up to 1 cm thick occur at some vein–wall-rock interfaces (Fig. 4a) indicating bedding slip continued beyond bedding-parallel vein formation. Slickenside directions are at high angles to fold hinge-lines but may deviate up to 30° from quartz-fibre lineations in the bedded veins. They have different character to the associated bedded vein and their presence suggests that veins may have determined the subsequent bedding-slip positions within the layered sandstone and mudstone sequence.

The importance of interlayer slip at low metamorphic grade cannot be understated. Experimental investigations on chevron-folding have shown that thin layers with low contact strength tend to form chevrons (e.g. Ghosh 1968). Radiolaria in the hinges of chevron folds within thinly bedded cherts of the Franciscan were

undeformed except within 1 mm of the chert-shale contacts, indicating that interbed shear–slippage played a major role in the folding process (Johnson 1970, p. 296). Similarly, slip between beds was important in the development of a concentric-like fold in limestone of the New York Appalachians (Chapple & Spang 1974). Internal strain patterns deduced from calcite twin lamellae in the limestone were consistent with buckling of a thick isotropic layer but had lower than expected magnitudes. The low strains and the observed fold curvature were explained by slip displacements of 24 cm on bedding planes spaced at 30 cm; observed grooved and slickensided bedding surfaces were spaced at 15–30 cm.

CHEVRON FOLD DEVELOPMENT: A DISCUSSION

Folding mechanisms—modelling

Folding of a competent layer under pseudo-viscous conditions has been treated as three phases: (1) initial homogeneous deformation (layer-parallel shortening); (2) permanent buckling; and (3) subsequent homogeneous deformation (flattening) (Milnes 1971, Hudleston 1973). Fold morphology, cleavage–bedding relationships and internal strain within folded layers will vary depending on the relative contributions of these mechanisms during the folding process (cf. Boulter 1979, Gray 1981, Hudleston & Holst 1984). Geometric analyses of fold and cleavage in this paper suggest that the formation of chevron folds in sandstone is due to a combination of different deformation mechanisms including layer parallel shortening, flexural-slip, pressure solution and rigid-body rotation.

Various scenarios can be tested by comparing observed fold parameters such as interlimb angle, bedding–cleavage angles, internal layer strain (from Fry plots) and fold flattening strain (from $t'\alpha$ plots) with those calculated from simple computational modelling. Folding-simulation models adopting symmetrical chevron forms for simplicity illustrate cleavage–fold relationships with progressive fold development (Fig. 8). Three different fold development stages at limb dips of 10, 60 and 75° are shown. *Stage A* represents the transition from layer parallel shortening to buckling. *Stage B* represents fold lock-up and *stage C* represents the final stage. Bedding and cleavage traces are treated as passive markers utilizing angular relationships between lines in the deformed and undeformed states (e.g. $\cot\alpha' = \cot\alpha + \gamma$, Ramsay 1967, equation 3-71 and $\tan\theta' = (1/R)\tan\theta$, Ramsay 1967, equation 3-34; where α is the angle between a line and the shear direction in the undeformed state, α' is the angle between a line and the shear direction in the deformed stage, γ is the shear strain, θ is the angle between a linear marker and the principal X stretch direction in the undeformed state, θ' is the angle between a linear marker and the principal X stretch direction in the deformed state, and R is the strain ratio).

Strain reversal utilizing the mudrock layer strains has

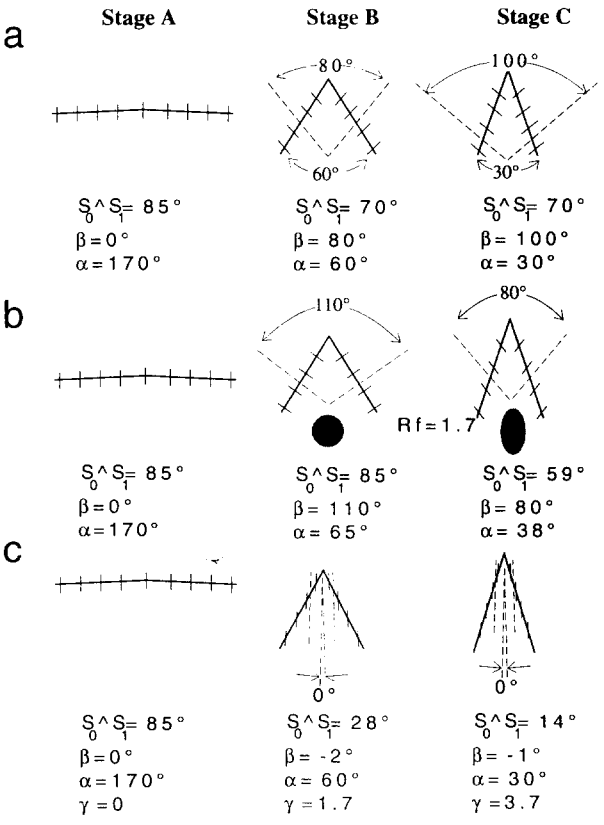

Fig. 8. Modelling of bedding–cleavage relationships at various stages in fold development. Stage A is the initial stage where the limb dip (θ) is 5° and the spaced cleavage is non-fanning. (a) Observed relationships based on data from Fig. 6 (b) Modelled sequence involving limb rotation and fold flattening; Stages A–B involve passive rotation of fold limbs and the spaced cleavage without change in the bedding–cleavage angle. Stages B–C involve homogeneous fold flattening with decreases in $S_0 \wedge S_1$ and in the cleavage fan angle. (c) Modelled sequence involving flexural-flow (intralayer distributed shear strain) within the sandstone; stages B and C show relationships for interlimb angles of 60 and 30°, respectively. α, fold interlimb angle; β, cleavage fan angle; γ, shear strain; R_f, fold flattening strain.

shown that the 'buckling' component of limb rotation is approximately 45° and the 'pure shear' (fold flattening) component is approximately 30° to give a final limb dip of 75° and the observed fold interlimb angle of 35° (see Gray & Willman 1991b, fig. 10). To achieve limb dips of 60–75° due to flexural-flow requires intrabed shear strains (γ) of 1.7–3.7 (see Ramsay 1967, fig. 7.57). An initial bedding–cleavage angle of 80° at a limb dip of 10° means that intrabed shear would produce a bedding–cleavage angle in the final state of 14° (i.e. where θ = 75°) (see Fig. 8c) (Ramsay 1967, equation 3.71). The fact that observed $S_0 \wedge S_1$ angles are >55° indicates that intrabed shear strain due to flexural-flow was not important in the sandstone layers during folding. Changes in $S_0 \wedge S_1$ during fold tightening must therefore be due to some other mechanism such as fold flattening.

Fold flattening values range from 1.4 to 1.8 (see Appendix 1). Assuming that fold flattening is important from limb dips (θ) of 55° then an homogenous flattening strain (R_f) of 1.7 would produce a new limb dip (θ') of 71° (i.e. an interlimb angle of 38°), a bedding–cleavage (ϕ) angle of 59° and a cleavage fan angle (β of 80° (Fig. 8). The modelled limb dip and bedding–cleavage angle match the observed values but the cleavage fan angle is

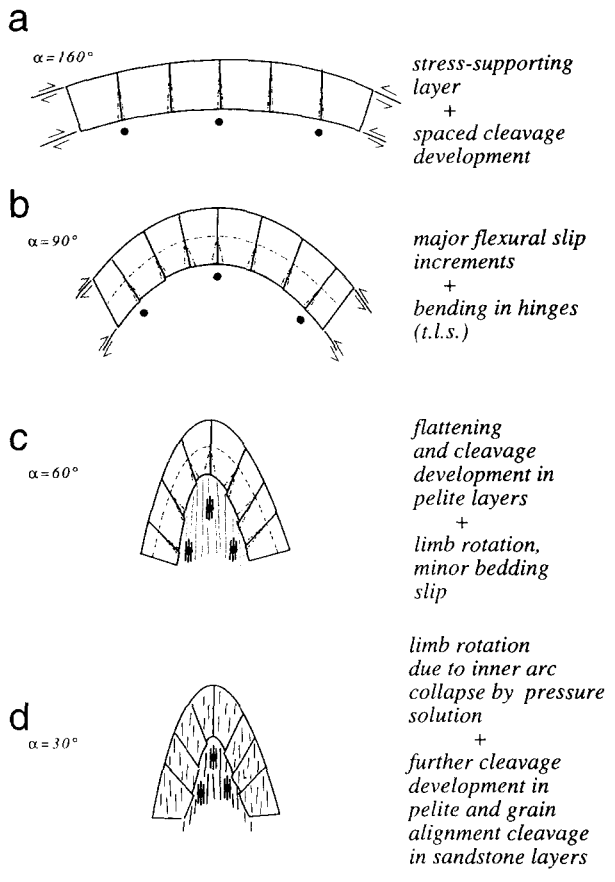

Fig. 9. Sequential development of chevron folds in a sandstone–mudstone multilayer sequence showing the varying influences of the sandstone and mudstone layers, respectively. Grey layer, mudstone; black circles, framboidal pyrites with straight fibrous quartz overgrowths in (c) and (d); dashed line; neutral surface within sandstone layer; α = interlimb angle; t.l.s., tangential longitudinal strain.

too low. This requires greater limb rotation than that expected solely from fold flattening.

Fold development scenario

Chevron folding in the examples described is the result of an interplay of processes not only within the sandstone layers but also in the intervening mudstone (Fig. 9). In the early stages the sandstone layers supported the stress within the multilayer with the resulting homogeneous strain due to layer-parallel shortening producing the spaced cleavage (Fig. 9a). Internal strain within sandstone at this stage is due to flattening and pressure solution. With the beginning of folding, flexural-slip was very important with little or no internal strain within sandstone layers (Fig. 9b). During folding sandstone layers experienced localized bending in hinge zones with a tangential longitudinal strain pattern superimposed on the early homogeneous strains; layer-parallel extension occurring in the outer arc with shortening on the inner arc. From limb dips of 45–60° the sandstone layers were passively rotated as mudstone layers underwent homogeneous shortening with development of a slaty cleavage (Fig. 9c). Folding reaches a threshold at an interlimb angle of 60° (De Sitter 1956, Ramsay 1974) with subsequent limb rotation and fold shape modification due to inner arc collapse by pressure solution and further enhancement of cleavage in the mudstone layers and development of a grain alignment cleavage superimposed on the early formed spaced cleavage (Fig. 9d).

CONCLUSIONS

(1) Development of chevron folds in a natural multilayer, where $t_1/t_2 \approx 1$ (t_1 is the stiff and t_2 the weak layer thickness, respectively) and general bed thicknesses are ~1 m, is due to changing behaviour and deformation mechanisms in both stiff (sandstone) and weak (mudstone) layers during the folding process.

(2) Layer parallel shortening, interbed slippage, rigid body rotation, hinge deformation due to tangential longitudinal strain and fold flattening have all played a part in the development of these chevron folds.

(3) Layer parallel shortening in sandstone was important in the pre-buckling stage with early development of a spaced cleavage and little or no internal strains between spaced cleavages.

(4) Interbed slippage was critical in the buckling stage and movement horizons appear to be controlled by positions of previously formed bedding-parallel veins.

(5) Intermediate stages in fold growth are dominated by passive limb rotation in sandstones and minor interbed slippage due to flattening and cleavage development in the intervening mudstones.

(6) Tightening of folds beyond 60° is caused by inner arc collapse due to pressure solution with enhancement of the spaced cleavage in sandstone and intensification of the cleavage in the mudrock. At this stage a grain alignment cleavage developed axial surface to folds overprinting the fanned spaced cleavage. XZ strains are up to 1.8 in fold hinges.

(7) Pressure solution played an important role in the folding process from early spaced cleavage initiation to late-stage geometric modification of fold shape with mica beard and grain alignment cleavage development.

(8) Chevron folding is part of a plane strain deformation involving no extension along the fold axis direction; micro-boudinaged opaques show subvertical extensions (X) of 10–32% but no segmentation in YZ sections (where X, Y and Z are, respectively, and maximum, intermediate and minimum principal axes of strain).

Acknowledgements—This study has been supported by grants from Visiting Fellowship Grant of Academia Sinica (awarded to X. Yang) and Australia Research Council Grants E8315675 and A39030706 (awarded to D. R. Gray). Yang thanks Clive Willman and Phonse Vandenberg for their help in field work, Robert Douglas for thin section making, and Steve Morton for photography. Stimulating discussions with Y. Zhang, J. Wang, S. C. Cox and C. Elliott have been proved very helpful for the research and paper writing. X. Yang expresses his acknowledgement for use of facilities in Department of Earth Sciences, Monash University, Melbourne, Australia, where the research and paper writing were conducted. Comments on the manuscript by P. G. Tanner and an anonymous reviewer helped to significantly improve the paper.

REFERENCES

Beutner, E. C. & Diegel, F. A. 1985. Determination of fold kinematics from syntectonic fibers in pressure shadows, Martinsburg Slate, New Jersey. *Am. J. Sci.* **285**, 16–50.

Boulter, C. A. 1976. Sedimentary fabrics and their relation to strain analysis methods. *Geology* **4**, 141–146.

Boulter, C. A. 1979. On the production of two inclined cleavages during a single folding event; Stirling Range, S.W. Australia. *J. Struct. Geol.* **1**, 207–219.

Chapple, W. M. & Spang, J. H. 1974. Significance of layer-parallel slip during folding of layered sedimentary rocks. *Bull. geol. Soc. Am.* **85**, 1523–1534.

Cox, S. F., Etheridge, M. A., Cas, R. A. F. & Clifford, B. A. 1991. Deformational style of the Castlemaine area, Bendigo–Ballarat zone: implications for evolution of crustal structure in central Victoria. *Aust. J. Ear. Sci.* **38**, 151–170.

Crespi, J. M. 1986. Some guidelines for the practical application of Fry method of strain analysis. *J. Struct. Geol.* **8**, 799–808.

De Sitter, L. U. 1956. *Structural Geology*. McGraw-Hill, New York.

Dieterich, J. H. & Carter, N. L. 1969. Stress history of folding. *Am. J. Sci.* **267**, 129–154.

Donath, F. A. & Parker, R. B. 1964. Folds and folding. *Bull. geol. Soc. Am.* **75**, 45–62.

Dunne, W. M., Onash, C. M. & Williams, R. T. 1990. The problems of strain-marker centres and the Fry method. *J. Struct. Geol.* **8**, 933–938.

Erslev, E. A. 1988. Normalized centre-to-centre strain analysis of packed aggregates. *J. Struct. Geol.* **10**, 201–209.

Fry, N. 1979. Random point distributions and strain measurement in rock. *Tectonophysics* **60**, 89–105.

Ghosh, S. K. 1968. Experiments of buckling of multilayers which permit interlayer gliding. *Tectonophysics* **6**, 207–249.

Gray, D. R. 1978. Cleavages in deformed psammitic rocks from southeastern Australia: their nature and origin. *Bull. geol. Soc. Am.* **89**, 577–590.

Gray, D. R. 1981. Cleavage–fold relationships and their implications for transected folds: an example from southeast Virginia, U.S.A. *J. Struct. Geol.* **3**, 265–277.

Gray, D. R. 1988. Structure and tectonics. In: *Geology of Victoria* (2nd edn) (edited by Douglas, J. G. & Fergusson, J. A.). Victn. Div. Geol. Soc. Aust., 1–36.

Gray, D. R. & Durney, D. W. 1979. Investigations on the mechanical significance of crenulation cleavage. *Tectonophysics* **58**, 35–79.

Gray, D. R. & Willman, C. E. 1991a. Deformation in the Ballarat Slate Belt, Central Victoria and implications for the crustal structure across southeast Australia. *Aust. J. Earth Sci.* **38**, 171–201.

Gray, D. R. & Willman, C. E. 1991b. Thrust-related strain gradients and thrusting mechanism in a chevron-folded sequence, southeastern Australia. *J. Struct. Geol.* **13**, 691–710.

Gray, D. R., Gregory, R. T. & Durney, D. W. 1991. Rock-buffered fluid–rock interaction in deformed quartz-rich turbidites sequences, Eastern Australia. *J. geophys. Res.* **96**, 19,681–19,704.

Groshong, R. H. 1975. Slip cleavage caused by pressure solution in a buckle fold. *Geology* **3**, 411–413.

Hanna, S. S. & Fry, N. 1979. A comparison of methods of strain deformation in rocks from southwest Dyfed (Pembrokeshire) and adjacent areas. *J. Struct. Geol.* **1**, 155–162.

Harris, A. L., Bradbury, H. J. & McGonical, M. H. 1976. The evolution and transport of the Tay nappe. *Scott. J. Geol.* **12**, 102–113.

Hudleston, P. J. 1973. An analysis of 'single layer' folds developed in a viscous media. *Tectonophysics* **16**, 189–214.

Hudleston, P. J. & Holst, T. B. 1984. Strain analysis and fold shape in a limestone layer and implications for layer rheology. *Tectonophysics* **106**, 321–347.

Jessell, M., Willman, C. E. & Gray, D. R. In press. Bedding parallel veins and their relationships to folding. *J. Struct. Geol.*

Johnson, A. M. 1970. *Physical Processes in Geology*. Freeman, Cooper & Co., San Francisco.

Johnson, A. M. 1977. *Styles of Folding. Developments in Geotectonics Series No.* 11. Elsevier, Amsterdam.

Lacassin, R. & Van den Driessche, J. 1983. Finite strain determination of gneiss: application of Fry method to porphyroid in the southern massif central (France). *J. Struct. Geol.* **5**, 245–253.

Means, W. H. 1975. Natural and experimental microstructures in deformed micaceous sandstones. *Bull. geol. Soc. Am.* **86**, 1221–1229.

Milnes, A. G. 1971. A model for analysing the strain history of folded competent layers in the deeper parts of orogenic belts. *Eclog. geol. Helv.* **64**, 335–342.

Mitra, S. 1978. Microscopic deformation mechanisms and flow laws in quartzites within the South Mountain anticline. *J. Geol.* **86**, 129–152.

Nakahara, D. K. & Wiltschko, D. V. 1986. Deformation in the hinge region of a chevron fold, Valley and Ridge Province, central Pennsylvania. *J. Struct. Geol.* **8**, 157–168.

Onasch, C. M. 1983. Origin and significance of microstructures in sandstones of the Martinsburg formation. *Am. J. Sci.* **283**, 936–966.

Onasch, C. M. 1986. Ability of the Fry method to characterize pressure-solution deformation. *Tectonophysics* **122**, 187–193.

Onasch, C. M. 1990. Microstructures and their role in deformation of a quartz arenite from the central Appalachian foreland. *J. Struct. Geol.* **12**, 883–894.

Paterson, M. S. & Weiss, L. E. 1966. Experimental deformation and folding in phyllite. *Bull. geol. Soc. Am.* **77**, 343–374.

Powell, C. Mc A. & Rickard, M. J. 1985. Significance of the early foliation at Bermagui, N.S.W., Australia. *J. Struct. Geol.* **7**, 385–400.

Ramsay, J. G. *Folding and Fracturing of Rocks*. McGraw-Hill, New York.

Ramsay, J. G. 1974. Development of chevron folds. *Bull. geol. Soc. Am.* **85**, 1741–1754.

Wu, S. & Groshong, R. H. 1991. Low-temperature deformation of sandstone, southern Appalachian fold–thrust belt. *Bull. geol. Soc. Am.* **103**, 861–875.

APPENDIX 1

Table A1. Table of fold data (see text for details)

Fold	Location	Map co-ordinates*	Basic shape	Fold type	Major rock type	Half-wavelength (m)	Interlimb angle (α) (°)	Cleavage fan angle (β) (°)	Fold flattening strain†
1	Castlemaine	BU536946	anticline	1B	sandstone	3	80	63	
2	Castlemaine	BU530941	anticline	1B	sandstone	5.8	80	62	1.4
3	Chewton	BU558926	anticline	3	mudrock	4.5	90	25	
4	Chewton	BU575915	anticline	1B	sandstone	3.8	89	72	
5	Lerderderg Gorge	BU718345	fold pair	1C	sandstone and mudrock	3	45	116	1.7
6	Lerderderg Gorge	BU715347	syncline	1C	sandstone and mudrock	2.8	40	80	1.6
7	Lerderderg Gorge	BU711353	fold pair	1C	sandstone and mudrock	5	50	86	
8A1	Steiglitz	BU477057	anticline	1C	sandstone	2.7	36	90	1.7
8A2	Steiglitz	BU477057	anticline	3	mudrock	2.7	36	58	
8S	Steiglitz	BU477057	syncline	1C	sandstone	2.4	52	42	1.8

*Map co-ordinates are from the Australian Map Grid for the Castlemaine (Map 7723) and Bacchus Marsh (Map 7722) 1:100,000 Topographic maps.

†Fold flattening strains were determined from photographs of fold profiles using a modified t'α method (see Gray & Durney 1979, pp. 60–65). Not all folds were suitable for flattening analysis.

APPENDIX 2

Table A2. Fry plot strain data from thin sections of sandstones (output from program 'Instrain': Erslev 1988). S_0 dip, dip of bedding; $S_0 \wedge S_s$, angle between bedding and spaced cleavage; $S_0 \wedge S_g$, angle between bedding and grain alignment cleavage; R, strain ratio determined from either vacancy ellipse or density ellipse; n, number of grain centres analysed; S_0, bedding; S_s, spaced cleavage; S_g, grain alignment cleavage.

Sample	S_0 dip	$S_0 \wedge S_s$	$S_0 \wedge S_g$	R	n	Ellipse type	Fabric description
Fold 1							
XY91-9C	40W	80°	40°	1.5	306	vacancy ellipse—S_0	weak seams—S_g
XY91-9B	5W	90°		1.5	282	vacancy ellipse—S_0	strong alignment elongate grains and detrital mica—S_0
				1.1	282	density ellipse—S_g	
XY91-9C	45E	85°	40°	1.6	244	vacancy ellipse—S_g	weak seams—S_g
Fold 2							
XY91-3A	20E	85°	65°	1.7	400	vacancy ellipse—S_g	strong grain alignment and strong mica fabric—S_g
XY91-3B	60W	75°	35°	1.4	261	vacancy ellipse—S_g	weak seams and mica fabric—S_g
XY91-3C	5W	85°	60°	1.6	400	vacancy ellipse—S_g	strong grain alignment and strong mica fabric—S_g
XY91-3D	64E	80°	40°	1.4	400	vacancy ellipse—S_g	strong grain alignment and strong mica fabric—S_g
Fold 4							
XY91-1A	18W	85°	45°	1.5	244	vacancy ellipse—S_g	weak seams—S_g
XY91-1B	74E	85°	45°	1.6	223	vacancy ellipse—S_g	weak seams and mica fabric—S_g
XY91-1C	50E	70°	70°	1.5	400	vacancy ellipse—S_g	weak seams and mica fabric—S_g
Fold 5							
XY91-6A	88W	80°	30°	1.7	328	vacancy ellipse—S_g	weak grain alignment and mica fabric—S_g
XY91-6B	20E	75°	55°	1.6	249	vacancy ellipse—S_0	some elongate grains—S_0
				1.8	249	density ellipse—S_g	weak grain alignment and mica fabric—S_g
XY91-6D	42E	53°	16°	1.5	204	vacancy ellipse—S_s	strong S_s, and mica fabric—S_g
XY91-6G	50E	70°	35°	1.4	303	vacancy ellipse—S_g	some elongate grains—S_0, weak mica fabric—S_g
XY91-6E	20W	80°	20°	1.7	237	vacancy ellipse—S_0	some elongate grains—S_0
				1.8	237	density ellipse—S_g	weak mica fabric—S_g
Fold 8							
XY91-7A	86W	70°	40°	1.7	243	density ellipse—S_g	some elongate grains—S_0 weak mica fabric—S_g
XY91-7B	90	80°	30°	1.8	321	vacancy ellipse—S_g	strong pressure solution fabric and weak mica fabric—S_g
XY91-7C	20E	70°	25°	1.6	253	vacancy ellipse—S_g	strong mica fabric 32% vertical extension from fractured opaques
XY91-7D	10W	80°		1.6	283	density ellipse—S_g	strong S_0 fabric
Overturned limb (see Fig. 2a for location)							
XY91-2A	85W	80°		1.7	388	vacancy ellipse—S_g	weak seams—S_g
XY91-2C	60W			1.8	379	vacancy ellipse—S_g	weak seams—S_g